Published online 31 May 2022

Nucleic Acids Research, 2022, Vol. 50, No. 15 ***e89***
https://doi.org/10.1093/nar/gkac434

A novel, rapid and sensitive flow cytometry method reveals degradation of promoter proximal paused RNAPII in the presence and absence of UV

Lilli T.E. Bay, Randi G. Syljuåsen and Helga B. Landsverk*

Department of Radiation Biology, Institute for Cancer Research, Norwegian Radium Hospital, Oslo University Hospital, 0379 Oslo, Norway

Received December 21, 2021; Revised April 08, 2022; Editorial Decision April 26, 2022; Accepted May 11, 2022

ABSTRACT

RNA polymerase II (RNAPII) is emerging as an important factor in DNA damage responses, but how it responds to genotoxic stress is not fully understood. We have developed a rapid and sensitive flow cytometry method to study chromatin binding of RNAPII in individual human cells through the cell cycle. Indicating enhanced transcription initiation at early timepoints, levels of RNAPII were increased at 15–30min after UV-induced DNA damage. This was particularly evident for the S5 phosphorylated form of RNAPII (pRNAPII S5), which is typically associated with promoter proximal pausing. Furthermore, degradation of pRNAPII S5 frequently occurs, as its levels on chromatin were strongly enhanced by the proteasome inhibitor MG132 with and without UV. Remarkably, inhibiting pause release with 5,6-dichloro-1-beta-ribo-furanosyl benzimidazole (DRB) further promoted UV-induced degradation of pRNAPII S5, suggesting enhanced initiation may lead to a phenomenon of 'promoter proximal crowding' resulting in premature termination via degradation of RNAPII. Moreover, pRNAPII S2 levels on chromatin were more stable in S phase of the cell cycle 2h after UV, indicating cell cycle specific effects. Altogether our results demonstrate a useful new method and suggest that degradation of promoter proximal RNAPII plays an unanticipated large role both during normal transcription and after UV.

INTRODUCTION

RNA polymerase II (RNAPII) transcribes DNA into mRNA and several non-coding RNAs (1). In addition, RNAPII plays a central role in the response to DNA damage. Cells are exposed to various forms of DNA damage from both endogenous and exogenous sources, and RNAPII is involved in detection, repair and signaling following such events (2–8). Understanding how RNAPII responds to DNA damage is therefore important to fully understand the DNA damage signaling and repair pathways, which are critical in human conditions such as cancer, neurodegenerative diseases, immune deficiencies, metabolic syndromes, ageing and infertility (9). DNA damage produced by ultraviolet radiation (UV) arrests the progression of elongating RNAPII (10). This arrest initiates transcription-coupled nucleotide excision repair (TC-NER) (2) and leads to a potent inhibition of transcription at the global level (11). Transcription resumption is required for cell survival after UV (12). Another global change to RNAPII after UV is its proteasome-mediated degradation (13). Elongating RNAPII is thought to be degraded as a 'last resort' mechanism to remove RNAPII when a block to transcription cannot be dealt with either by repair or bypass (14). However, whether degradation of other forms of RNAPII occurs after UV is not known.

The basal RNAPII transcription cycle includes recruitment and formation of the preinitiation complex at the promoter region, promoter release and stalling after ∼50 nts at the promoter proximal pause site, release from pausing into productive elongation, and finally termination. Release from promoter proximal pausing into productive elongation is considered a main rate-limiting step of transcription (15). In addition, premature termination from the promoter proximal pause site or during productive elongation is common and limits pervasive transcription (16–18). Terminating RNAPII is thought to be recycled for new rounds of transcription (19). In its C-terminal domain (CTD), RPB1 (hereafter referred to as RNAPII), the largest subunit of RNAPII, contains a large non-structured domain, which in humans is made up of 52 heptapeptide aminoacid repeats that can undergo extensive post-transcriptional modifications. These modifications are involved in all stages of the transcription cycle and in RNA metabolism (20). The most studied modifications are phosphorylation of serine 5 (pRNAPII S5) and serine 2 (pRNAPII S2). While pRNAPII S5 is high in pro-

*To whom correspondence should be addressed. Tel: +47 22781462; Fax: +47 22781495; Email: heblan@rr-research.no

moter proximal regions, pRNAPII S2 is associated with productive elongation (20). Global levels of pRNAPII S5 and pRNAPII S2 can therefore be used as markers for the promoter proximal and productively elongating fractions respectively. Proteasome-mediated degradation of RNAPII occurs even in the absence of DNA damage, and is thought to positively affect the rate of transcription by removing stalled RNAPII complexes (21). As pRNAPII S5 was shown to strongly inhibit ubiquitination and proteasome mediated degradation, promoter proximal paused RNAPII has been assumed to be refractory to degradation (21). On the other hand, binding between a E3 ubiquitin ligase complex and pRNAPII S5 was enhanced after UV (22), suggesting pRNAPII S5 may play multiple roles in RNAPII degradation after UV.

Cell cycle progression is highly regulated by RNAPII-mediated transcription, as transcription of specific cell cycle genes is required for transition from one cell cycle phase into the other (23). Conversely, the cell cycle regulates RNAPII. This is evident in mitosis, when most of RNAPII and many transcription associated proteins are lost from chromatin through a process known as mitotic inhibition of transcription (24–26). RNAPII is also regulated by replication during S phase. Sharing the same template, RNAPII can create a physical barrier for DNA replication (27). Resulting transcription–replication conflicts (T–R conflicts) can cause replication stress, and are actively suppressed by evicting RNAPII from chromatin (28), by its degradation on chromatin (29). In line with a negative role for T–R conflicts in regulation of transcription, the level of transcription of a specific gene is lower during its time of replication (30). Promoter proximal sites also tend to be under-replicated during S phase, indicating that the presence of RNAPII at the promoter proximal region creates a hindrance for DNA replication (30). Moreover, UV affects the cell cycle as it strongly suppresses DNA replication (31) and activates cell cycle checkpoints (32). Nevertheless, it is not known how UV impacts RNAPII levels on chromatin through the cell cycle.

Techniques to study the RNAPII transcription cycle after UV include chromatin immunoprecipitation followed by sequencing (ChIP-seq) (33,34), GRO-seq (11) or nascent RNA-seq (34), chromatin fractionation followed by western blotting (35) or mass spectrometry (36) and live cell microscopy of endogenous GFP-RNAPII (37,38). These complementary techniques have provided major insights into the effect of UV on RNAPII-mediated transcription. However, although sequencing or chromatin fractionation techniques can give high resolution sequence information and/or quantitative data, they have so far been based on cell lysates made from a large number of pooled cells. To study cell cycle effects with these methods, cells must therefore be synchronized, which, depending on the synchronization method, may induce replication stress or changes to transcription. On the other hand, live cell microscopy gives spatial information and single cell resolution, but is limited in the number of cells analyzed, and does not easily allow the analysis of modifications on RNAPII. There is therefore a need for additional methods to study RNAPII chromatin levels in individual cells. Here, we describe a new rapid, quantitative and sensitive flow cytometry method to study RNAPII chromatin binding in individual cells through the cell cycle. Using this method we show that promoter proximal paused RNAPII is subject to proteasome-mediated degradation in the presence and absence of UV-induced DNA damage. Moreover, productively elongating RNAPII becomes more stable in S phase after UV, in line with TC-NER specific effects in replicating cells. Finally, as pRNAPII S5 was more removed in early S phase compared to G1 phase after suppression of release into productive elongation by 5,6-dichloro-1-beta-ribo-furanosyl benzimidazole (DRB), this suggests T–R conflicts are likely dealt with by degrading promoter proximal RNAPII.

MATERIALS AND METHODS

Cell culture

Human female cervical cancer HeLa Kyoto cells were cultivated in Dulbecco's modified Eagle's medium (DMEM) and human male SV40-transformed fetal lung fibroblast MRC5 and human non-transformed retinal pigment epithelial (RPE) cells were cultivated in DMEM:Nutrient Mixture F-12 at 37°C in a humidified environment with 20% O_2 and 5% CO_2. Both mediums were supplemented with 10% fetal bovine serum (VWR, Biowest) and 1% Penicillin/Streptomycin (ThermoFisher Scientific). HeLa Kyoto (HeLa) cells were used throughout the manuscript unless otherwise stated.

Chemicals and treatments

UV- irradiation was performed with an UVC crosslinker (UV Stratalinker 2400 (Stratagene)) at 20 J/m^2. DRB (Sigma Aldrich) was used at 100 μM, EdU (Thermo Fisher) at 1 μM, CDK7-inhibitor THZ1 (ApexBio) at 1 μM, MG132 (Sigma Aldrich) at 50 μM, and Nocodazole (Sigma Aldrich) at 1 μg/ml.

Western blotting—chromatin fractionation and antibodies

Cells were harvested and washed with PBS. To release soluble factors, the cell pellet was resuspended in ice-cold chromatin extraction buffer (20 mM HEPES (pH 7.9), 1.5 mM $MgCl_2$, 140 mM NaCl, 300 mM Sucrose, 0.5% TX-100, Complete EDTA-free Protease Inhibitor Cocktail (Merck), PhosSTOP phosphatase inhibitors (Merck) and 20 μM MG132 (Sigma Aldrich). The cell pellet was incubated in the extraction buffer for 5min at 4°C with gentle mixing (300 rpm), and soluble and chromatin bound fractions were separated by centrifugation. The chromatin bound pellet was washed once in extraction buffer, followed by chromatin digestion with 100 U/ml benzonase (Sigma Aldrich) in extraction buffer for 2h at 4°C with gentle mixing (300 rpm). Both soluble and chromatin bound fractions were added Lane Marker Reducing Sample Buffer (Pierce Biotechnologies) and boiled at 95°C prior to analysis by quantitative western blotting. The final volumes of chromatin bound and soluble fractions were kept equal to allow comparison of the two fractions. Criterion TGX Stain-free gels (Bio-Rad) and nitrocellulose membranes (BioRad) were used for separation and transfer respectively. Criterion Stain-free imager was activated in a Chemidoc MP (BioRad) prior to

transfer. Antibodies used were: total RNAPII (F-12, Santa Cruz Biotechnologies), pRNAPII S5 (3E8) and pRNAPII S2 (3E10) (Sigma Aldrich). Total protein levels obtained from stain-free signal on membranes were used as loading control. Blots were imaged using chemiluminescence substrates (Supersignal west pico, dura or femto from Thermo Scientific). The Image Lab 4.1 (BioRad) software was used for quantifications and processing of images. Saturated signals were excluded. For accurate quantifications, a dilution curve of one of the samples was included. Membranes were stripped using ReBlot Plus Mild Antibody Stripping Solution (Millipore) in order to allow a new round of blotting for proteins.

Isolation of mitotic cells

For analysis of mitotic cells, cells were synchronized by 1 μg/ml nocodazole treatment 16h prior to harvest. The mitotic fraction was further isolated through mitotic shake off by gently tapping the dish in order to loosen mitotic cells. Cells floating in the medium were next transferred to a tube and isolated by centrifugation. For western blotting, cells were counted and cell number was adjusted in order to directly compare chromatin association of RNAPII in mitosis vs interphase. Chromatin fractionation was performed as described above.

Chromatin fractionation for flow cytometry

To release unbound factors, isolated cell pellets were resuspended in 100 μl chromatin extraction buffer for 5min on ice. For the experiments performed to optimize extraction strength, different concentrations of NaCl in the chromatin extraction buffer were tested: 50, 140, 180, 220, 280 mM, for all other experiments, 140 mM NaCl was used. Following extraction, cells were fixed by addition of 900 μl 10% formalin solution (Sigma Aldrich), and left at room temperature for 10min. Cells were then resuspended in PBS, followed by barcoding and antibody staining as described below.

Flow cytometry analysis

In all flow cytometry experiments, antibody staining and barcoding was performed as previously described (29,39). Flow cytometry analysis was performed on a LSRII flow cytometer (BD Biosciences) using Diva and FlowJo software. 10 000 cells or more were analyzed per sample, per experiment, including barcoding cells.

In brief, non-treated HeLa cells were incubated with 0.002 μg/μl Alexa Fluor 647 Succinimidyl Ester (Thermo Fisher) in PBS for 30min prior to antibody staining. In most experiments the barcoded control consisted of extracted cells, with the exception of the salt concentration optimization experiments where the barcoded control was non-extracted. Barcoding was quenched by addition of PBS with 5% fetal bovine serum (FBS (Biowest)). Thereafter, the barcoded cells were distributed equally among all the samples prior to staining as described below. For co-staining with pH3S10 and RNAPII, pRNAPII S5 or pRNAPII S2, cells were incubated with primary (anti-pH3S10 (Millipore) and anti-RNAPII (D8L4Y, Cell Signaling Technology)), anti-pRNAPII S5 (3E8) or anti-pRNAPII S2 (3E10) (Sigma Aldrich) and secondary antibodies (anti-mouse Alexa Fluor 568 and anti-rabbit (RNAPII) or anti-rat Alexa Fluor 488 (pRNAPII S5 and pRNAPII S2) Thermo Fisher), diluted in flow buffer (0.1% Igepal CA-630, 6.5 mM Na_2HPO_4, 1.5 mM KH_2PO_4, 2.7 mM KCl, 137 mM NaCl, 0.5 mM ethylenediaminetetraacetic acid (pH 7.5)) containing 4% non-fat milk. Samples were next stained with the DNA-stain Hoechst 33258 (1.5 μg/ml (Sigma Aldrich)) in flow buffer and analyzed by flow cytometry. As endogenous RNAPII was tagged with GFP, for MRC5 cells, staining for anti-pRNAPII S5, S2 or anti-pH3S10 was followed by anti-rat or mouse Alexa Fluor 568. For experiments with EdU incorporation, cells were labeled with 1 μM EdU for 1h prior to further 2h treatment with UV or inhibitors, resulting in a maximal EdU incorporation of 3h. The relatively long incubation with EdU was to ensure that all cells that had gone from G1 into S during the course of the treatments were correctly gated as EdU positive S phase cells. On the other hand, the long EdU incubation may have caused some cells gated as late S to actually be G2 cells that had stopped replicating during the course of the treatment. After EdU incorporation and treatments, samples were harvested and subjected to chromatin fractionation for flow cytometry (see above), barcoded (as described above) and labeled with primary (anti-RNAPII (D8L4Y, Cell Signaling Technology), anti-pRNAPII S5 (3E8) or anti-pRNAPII S2 (3E10) (Sigma Aldrich)) and secondary antibodies (Alexa Fluor 488, anti-rabbit for RNAPII and anti-rat for pRNAPII S5 and S2 (Thermo Fisher)). Following this, EdU was labeled with the Click-iT Plus EdU Alexa Fluor 594 Flow Cytometry Assay Kit (Thermo Fisher), and DNA was stained with Hoechst 33258 (1.5 μg/ml(Sigma Aldrich)) in flow buffer. The rationale for gating of the cell cycle phases was the following (See also Figure 1F). G1 cells were negative for EdU, and had a G1 DNA content. Early S phase cells had close to G1 DNA content but were EdU positive. Mid S had an intermediary DNA content and were EdU positive. Late S phase cells had approximately a G2 DNA content, but were EdU positive. G2 cells were EdU negative and had a G2 DNA content. Mitotic cells formed the small population below the G2 cells (see Figure 1F—this was verified by low RNAPII staining (results not shown)) and were not included in the analysis of 'G2 cells'.

Immunofluorescence analysis

RNAPII loading was measured by immunofluorescence microcopy in either non-extracted or chromatin-extracted HeLa cells. For detection of chromatin-bound RNAPII, cells were incubated in chromatin extraction buffer for 5min on ice prior to 12min fixation with formalin solution (Sigma Aldrich) at room temperature. Coverslips were stained with anti-pH3S10 (Millipore) in combination with either anti-RNAPII (D8L4Y, Cell Signaling Technology), anti-pRNAPII S5 (3E8) or anti-pRNAPII S2 (3E10) (Sigma Aldrich) in PBS-AT (PBS with 0.5% Triton X-100 and 1% BSA), followed by anti-mouse Alexa Fluor 568 and anti-rabbit Alexa Fluor 488 (for RNAPII) or anti-rat Alexa Fluor 488 (for pRNAPII S5 and S2) (Thermo Fisher). DNA was stained with Hoechst 33342 (Sigma Aldrich) and cover-

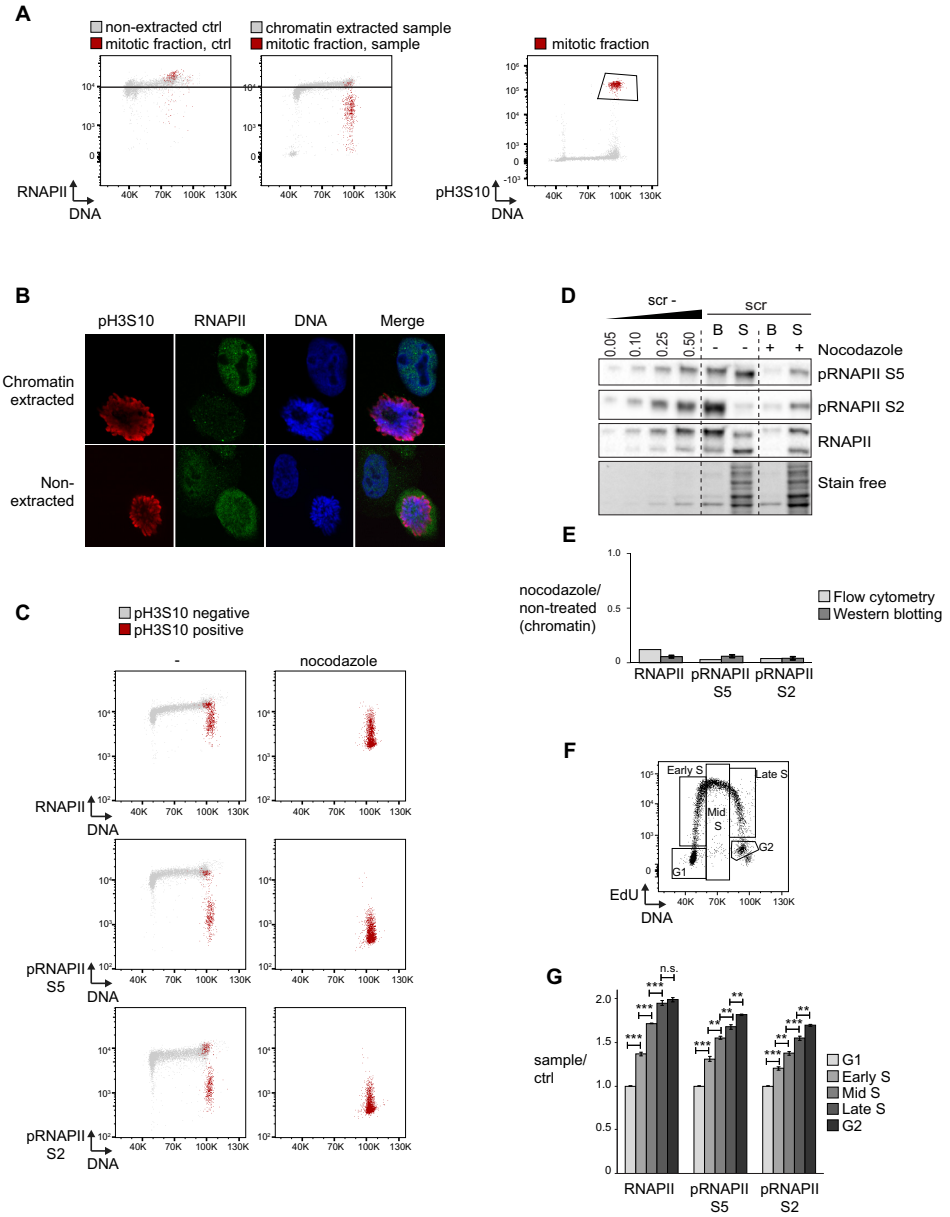

Figure 1. A new method to accurately measure RNAPII chromatin loading in individual cells through the cell cycle. (**A**) Flow cytometry scatter plots showing chromatin extracted (140 mM NaCl) or non-extracted cells labeled with antibodies against the N-terminal domain of RNAPII and the mitotic marker phosphorylated histone H3 on Serine 10 (pH3S10) relative to DNA content. The mitotic cells were gated as shown in the pH3S10 plot to the right, and shown in red in the RNAPII plots to the left. RNAPII staining was lost from chromatin in mitosis in the chromatin extracted, but not in the non-extracted cells. (**B**) Immunofluorescence analysis of chromatin extracted (140 mM NaCl) or non-extracted cells using antibodies to RNAPII and pH3S10. DNA was stained with Hoechst 33342. (**C**) Flow cytometry scatter plots of chromatin extracted non-treated (−) and nocodazole synchronized (nocodazole) HeLa cells. Non-treated cells were barcoded and mixed with mitotic cells synchronized by mitotic shake off after nocodazole treatment for 16h. Samples were stained with antibodies against total RNAPII, or phosphorylated serine 2 or 5 on the carboxyterminal domain of RNAPII combined with antibodies against pH3S10 and separated during analysis. pH3S10 negative cells are shown in grey and pH3S10 positive cells are shown in red in the respective non-treated and nocodazole synchronized cells. Note that, as expected, all the cells were pH3S10 positive in the nocodazole synchronized condition, and thus there are no observable pH3S10 negative cells. (**D**) Western blot analysis of chromatin bound (B) and soluble (S) fractions after extraction of non-treated and nocodazole synchronized cells as in (C). Cells were counted prior to extraction, and equal amounts of cells were loaded per lane. Stain free signal (BioRad Technologies), indicating total protein loading, was used as loading control. (**E**) Median chromatin levels of RNAPII, pRNAPII S5 and pRNAPII S2 in nocodazole treated sample divided by median chromatin levels in the non-treated ctrl (grey + red), obtained by flow cytometry analysis as in (C), compared to chromatin levels obtained in similar samples by western blotting as in (D). Notably, levels in dilution curve (as in (D)) were used for accurate quantification by western blot. ($n = 3$ for western blot samples). (**F**) Flow cytometry scatter plot of EdU incorporation relative to DNA content in HeLa cells. 1 μM EdU was added 3h prior to harvest. The cell cycle phases G1, early S, mid S, late S and G2 were determined based on EdU levels versus DNA content as shown. (**G**) Mean median RNAPII, pRNAPII S5 and pRNAPII S2 chromatin levels in individual phases of the cell cycle in HeLa cells. Alexa Fluor 647 barcoded, chromatin extracted control cells (that were not EdU treated) were added to each individual sample prior to staining. These were separated from the sample cells during analysis (Supplementary Figure S1B). Thereafter, median RNAPII, pRNAPII S5 and pRNAPII S2 levels in individual cell cycle phases were normalized to median levels in the barcoding cells to minimize sample to sample variation. Furthermore, each cell cycle phase was compared to G1, which was set to 1 ($n = 3$) *P*-values were determined by the two-tailed one sample *Student's* t-test. Error bars represent SEM.

slips were mounted onto a microscopy slide using Prolong Diamond (Thermo Fisher). Imaging and analysis was performed as previously described (29).

RESULTS

A new method to accurately measure RNAPII chromatin loading in individual cells through the cell cycle

To optimize a flow cytometry method accurately determining RNAPII levels on chromatin in individual cells through the cell cycle, we took advantage of the loss of RNAPII from chromatin in mitosis (40). To visualize mitotic cells, we co-stained RNAPII with the mitotic marker phosphorylated Histone H3 on Serine 10 (pH3S10). Chromatin extraction was performed using a mild detergent (0.5% TX-100) with various NaCl concentrations (Supplementary Figure S1A). Barcoding with non-extracted control HeLa cells was used as an internal standard for accurate quantifications and to determine extraction strength (Supplementary Figure S1A, B). As expected, mitotic cells clearly showed lower RNAPII staining after extraction with 140 mM NaCl and above (Figure 1A and Supplementary Figure S1A). However, in non-extracted cells, RNAPII levels in mitotic cells were similar to interphase cells with a G2 DNA content (Figure 1A). Notably, some of the extracted pH3S10 positive cells had high RNAPII staining (Figure 1A, C and Supplementary Figure S1A). The high RNAPII staining in a fraction of the pH3S10 positive cells remained even after extraction with increasing NaCl concentrations (Supplementary Figure S1A), showing it was not due to insufficiently strong extraction conditions. High pH3S10 levels thus likely occurs prior to loss of RNAPII from chromatin at the G2 to M transition. We chose to continue our experimental work with 140 mM NaCl, as it is close to physiological conditions and the chromatin levels of RNAPII were clearly lower in the mitotic fraction (Figure 1A). Analysis of the GFP signal in MRC5 cells expressing knock-in GFP tagged RNAPII (38) verified that the pattern of RNAPII antibody staining corresponded to endogenous RNAPII levels (Supplementary Figure S1C). The mitotic vs interphase RNAPII staining pattern after extraction with detergent and 140 mM NaCl was also confirmed by immunofluorescence microscopy (Figure 1B). To validate that the flow cytometry technique could be used to accurately quantify RNAPII levels on chromatin, we compared RNAPII levels in nocodazole-synchronized mitotic cells measured by flow cytometry versus quantitative western blotting. Similar levels of RNAPII on chromatin were observed using the two techniques (Figure 1C–E). Antibodies against pRNAPII S5 and pRNAPII S2 also showed low chromatin staining of mitotic cells (Figure 1C and Supplementary Figure S1D, E) and similar chromatin levels were found using flow cytometry vs quantitative western blotting (Figure 1C–E). As RNAPII is involved in S phase specific events, such as T–R conflicts, we next addressed whether we could measure RNAPII chromatin levels in finely separated cell cycle transitions by including EdU incorporation to mark replicating cells. Gradually increasing RNAPII, pRNAPII S5 and pRNAPII S2 levels could be detected in cells from G1 to early-, mid- and late S and G2 phases (Figure 1F, G). The increasing levels of RNAPII on chromatin through the cell cycle were expected, as the cells grow and the DNA is duplicated. Of note, we also assessed chromatin bound RNAPII and pRNAPII S5 in a previous study (29), but in that work we did not include cell cycle analysis and did not fully optimize and validate the method. Based on the results shown here, we conclude that our novel flow cytometry method can be used to accurately measure RNAPII levels on chromatin in individual cells through the cell cycle.

Initiation is likely enhanced at early timepoints after UV irradiation

Using our new technique, we addressed changes in RNAPII levels on chromatin after UV irradiation. Higher levels of all forms of RNAPII were observed at early timepoints (15 and 30min) after UV in HeLa cells, especially in G1 phase of the cell cycle (Figure 2A–D and Supplementary Figure S2A). This effect was most pronounced for pRNAPII S5 (Figure 2B–D), in line with enhanced initiation causing more promoter proximal pausing at early timepoints after UV. Higher levels of pRNAPII S5 were also observed at 30min after UV in RPE cells (Figure 2E). Moreover, slightly higher levels of pRNAPII S2 could also be observed at 30min after UV in HeLa cells (Figure 2D), consistent with accompanying increased productive elongation. At 2h after UV, RNAPII and pRNAPII S5 were reduced, but pRNAPII S2 remained high in HeLa cells (Figure 2B–D). In this cell line, pRNAPII S2 is thus more long-lived than pRNAPII S5 after UV. Furthermore, chromatin binding of pRNAPII S5 was clearly lower in S phase compared to G1 and G2 phases at 2h after UV in HeLa cells (Figure 2F). Less pronounced cell cycle effects were observed at 15 and 30min, although the pRNAPII S5 levels again were slightly lower in S phase compared to G1 (Supplementary Figure S2B, C). pRNAPII S5 may therefore be more removed in S phase after UV in HeLa cells. The latter is likely a cell line dependent effect as pRNAPII S5 was not lower in S versus G1 phase after UV in RPE cells (Supplementary Figure S2D,E). On the other hand, levels of pRNAPII S2 were higher in S versus G1 phase 2h after UV in both HeLa and RPE cells (Figure 2F and Supplementary Figure S2D), indicating the productively elongating fraction may become more stable in S phase after UV. Higher stability of pRNAPII S2 in S phase at 2h after UV was also observed in MRC5 cells (Supplementary Figure S2F). Enhanced initiation causing more promoter proximal pausing at early timepoints, and higher stability of the elongating RNAPII fraction in S phase, thus likely represent general phenomena after UV.

pRNAPII S5 is degraded on chromatin in the presence and absence of UV

To address whether cell cycle phase differences in RNAPII chromatin binding after UV might be caused by changes in RNAPII degradation on chromatin, we added the proteasome inhibitor MG132. RNAPII and pRNAPII S5 levels were enhanced on chromatin after MG132 (Figure 3A–C) in an unperturbed cell cycle in HeLa cells, as previously observed (29). Enhanced levels of pRNAPII S5 on chromatin after treatment with MG132 were also observed in RPE cells (Figure 3D). pRNAPII S2 levels were less enhanced by

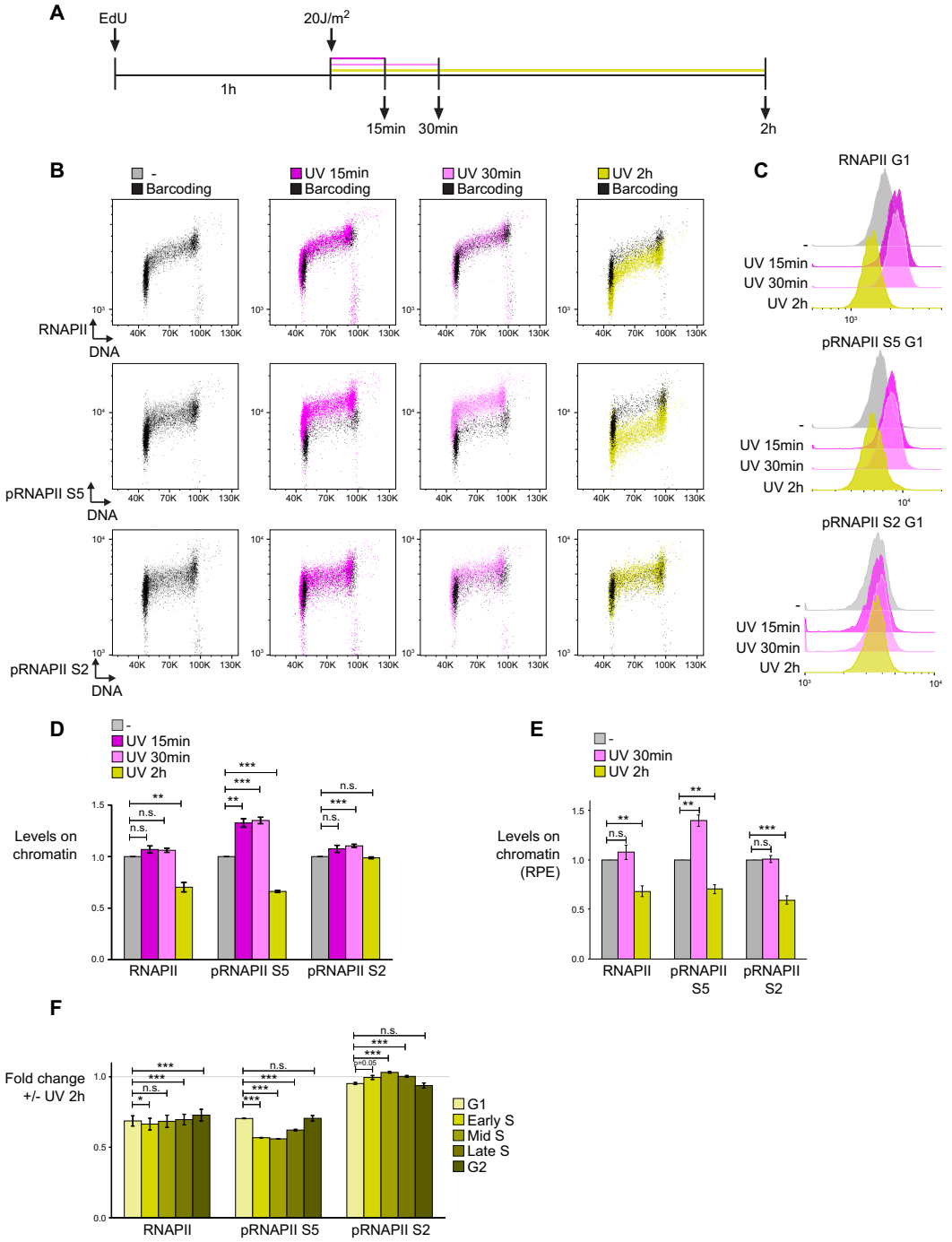

Figure 2. Initiation is likely enhanced at early timepoints after UV irradiation. (**A**) Overview of experimental set up. EdU was added to HeLa cells 1h prior to UV irradiation with 20 J/m^2. Samples were harvested, extracted and fixed for flow cytometry analysis at 15min, 30min and 2h after UV. Non-UV irradiated cell samples were harvested together with the UV 2h cell samples. (**B**) Flow cytometry scatter plots showing levels of RNAPII, pRNAPII S5 and pRNAPII S2 on chromatin versus DNA content from samples treated as in (A). Non-UV irradiated cells (−) are shown in grey, and samples harvested at 15min (UV 15min), 30min (UV 30min), and 2h after UV (UV 2h) in colors as indicated. Barcoded control cells (shown in black) were added to all individual samples prior to staining, separated from the samples during analysis (as in Figure 1G), and shown in scatterplots together with the sample cells. Note that in the non-UV irradiated (−) sample the barcoding cells (black), largely overlap with sample (grey), but in the UV treated samples the sample cells are frequently shifted either higher or lower than the barcoding cells, showing that the chromatin levels of RNAPII, pRNAPII S5 and pRNAPII S2 change after UV. (**C**) Flow cytometry histograms showing RNAPII, pRNAPII S5 and pRNAPII S2 levels on chromatin vs cell count in individual G1 cells (determined as in Figure 1F). (**D**) Mean median RNAPII, pRNAPII S5 and pRNAPII S2 levels on chromatin in cells treated as in A) and normalized to barcoding cells. UV-treated samples were further normalized to non-treated sample ($n = 3$), significance tested by the two-tailed one sample *Student's* test. Error bars represent SEM. **(E)** Mean median RNAPII, pRNAPII S5 and pRNAPII S2 levels on chromatin in RPE cells treated as in A) and analyzed as in D) ($n = 3$), significance tested by the two-tailed one sample *Student's* test. Error bars represent SEM. (**F**) Mean fold changes 2h after UV of RNAPII, pRNAPII S5 and pRNAPII S2 levels on chromatin in individual phases of the cell cycle (determined as in Figure 1F), and normalized to barcoding cells. ($n = 3$), significance tested by the two-tailed one sample *Student's* test. Error bars represent SEM.

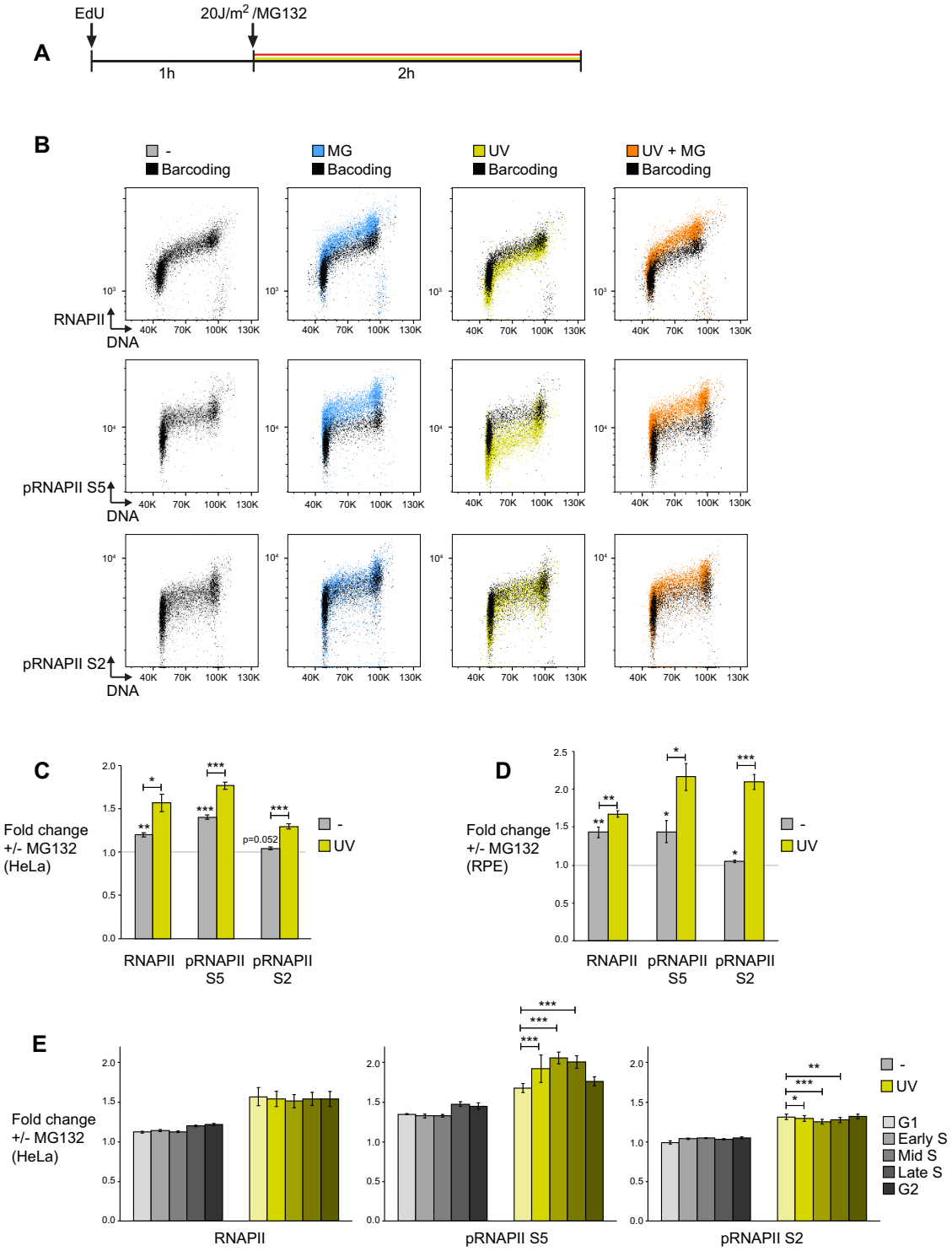

Figure 3. pRNAPII S5 is degraded on chromatin in the presence and absence of UV. (**A**) Overview of experimental set up. EdU was added to HeLa cells 1h prior to UV irradiation with 20 J/m^2 and addition of 50 μM MG132. Samples were harvested, extracted and fixed for flow cytometry analysis at 2h after UV/ addition of MG132. (**B**) Flow cytometry scatter plots showing levels of RNAPII, pRNAPII S5 and pRNAPII S2 on chromatin versus DNA content from samples treated as in A). Non-treated cells (−) are shown in grey, and samples treated with UV and/or MG132 are shown in colors as indicated. Barcoded control cells (shown in black) are shown in scatterplots together with the sample cells as in Figure 2B. (**C**) Mean fold changes after MG132 treatment (chromatin levels with MG132 / chromatin levels without MG132) in the presence (yellow) or absence (grey) of UV, from experiments as in B). Note that even in the absence of UV, the mean fold change after MG132 is above 1 (meaning MG132 increases the chromatin binding) for RNAPII and pRNAPII S5, but less so for pRNAPII S2. After UV, the average fold changes for all the RNAPII forms are increased. ($n = 3$), significance tested by the two-tailed one sample Student's *t*-test. Error bars represent SEM. (**D**) As in C) except showing fold changes after MG132 in RPE cells. ($n = 3$), significance tested by the two-tailed one sample *Student's t*-test. Error bars represent SEM. (**E**) Mean fold changes after MG132 treatment (as in C) in individual phases of the cell cycle (determined as in Figure 1F). ($n = 3$), significance tested by the two-tailed one sample Student's *t*-test. Error bars represent SEM.

MG132 treatment alone both in HeLa and RPE cells (Figure 3B–D), suggesting the productively elongating fraction is less degraded under unperturbed conditions. After UV, proteasome mediated degradation of all forms of RNAPII was enhanced both in HeLa and in RPE cells (Figure 3B–D). Notably, the enhanced degradation of pRNAPII S5 after UV was unexpected, as promoter proximal RNAPII has been thought to avoid degradation with and without UV (21,41). In addition, proteasome mediated degradation of pRNAPII S5 was higher in S phase versus G1 phase after UV in HeLa cells (Figure 3E), showing that the lower levels of pRNAPII S5 in S phase vs G1 at 2h after UV (Figure 2F) were caused by increased degradation (more removal). On the other hand, pRNAPII S2 was less degraded in S versus G1 phase both in HeLa cells and in RPE cells after UV (Figure 3E, Supplementary Figure S3A), in line with the higher stability of the elongating RNAPII fraction in S phase after UV (Figure 2F, Supplementary Figure S2D, F).

Promoter proximal RNAPII is subjected to proteasome-mediated degradation on chromatin in unperturbed conditions

Our results with pRNAPII S5 using MG132 suggested proteasome-mediated degradation of promoter proximal paused RNAPII occurs on chromatin under non-perturbed conditions. We hypothesized that enhancing promoter proximal pausing might increase RNAPII degradation. To address this, we added the widely used transcriptional inhibitor DRB, which prevents the release of RNAPII from the promoter proximal pause site into productive elongation (42). Several recent ChIP-seq experiments have confirmed that DRB causes a widespread arrest of RNAPII at the 5′ end of genes (43–45), though a few DRB-insensitive genes have also been reported (46). As expected, levels of pRNAPII S2 were decreased and levels of pRNAPII S5 were increased after treatment with DRB (Figure 4A–D). Moreover, in line with our hypothesis, total RNAPII chromatin levels were lower after DRB, and were completely reversed with MG132 (Figure 4A-D). Strongly supporting that proteasome-mediated degradation of the promoter proximal form of RNAPII was responsible for the lower levels of RNAPII on chromatin after DRB, the levels of pRNAPII S5, but not pRNAPII S2, were greatly enhanced by DRB + MG132 (Figure 4B–D). Moreover, pRNAPII S5 chromatin binding was lower in early S phase compared to G1 phase after DRB treatment (Figure 4E), suggesting enhanced promoter proximal RNAPII pausing by DRB causes more degradation of RNAPII in early S phase. As the majority of actively transcribing chromatin is early replicating (47), the distinct effects in early S vs G1 suggest that transcription replication conflicts involving promoter proximal RNAPII may be dealt with by degrading RNAPII.

Promoter proximal RNAPII is subjected to proteasome-mediated degradation on chromatin after UV

Enhanced levels of pRNAPII S5 on chromatin after UV and MG132 (Figure 3) suggested promoter proximal RNAPII may be subjected to proteasome-mediated degradation also after UV. However, productively elongating RNAPII is widely considered to be the form that is degraded after UV (21,41). We reasoned that if the productively elongating form was the only form that was degraded after UV, then inhibiting productive elongation should globally suppress UV-mediated degradation of RNAPII. To address this, we added DRB prior to UV treatment. Remarkably, RNAPII and pRNAPII S5 were more removed from chromatin after co-treatment with DRB and UV compared to either UV or DRB treatment alone (Figure 5A–C). Furthermore, MG132 reversed the lower levels of RNAPII and pRNAPII S5 after DRB and UV (Figure 5B, C), indicating proteasome-mediated degradation. UV-mediated degradation of RNAPII thus does not depend upon productive elongation. Rather, our results suggest that the promoter proximal form of RNAPII is degraded after UV. As expected, productive elongation was inhibited after DRB treatment, as levels of pRNAPII S2 were lower both with and without UV or MG132 (Figure 5B-C). Moreover, continuous release of RNAPII into productive elongation was required for maintenance of high pRNAPII S2 levels on chromatin 2h after UV in HeLa cells (Compare UV to UV + DRB, Figure 5B, C). Notably, co-treatment with DRB and UV caused a greater reduction in pRNAPII S2 than DRB alone (Figure 5B, C). This is likely due to UV- mediated degradation of productively elongating RNAPII that was either ongoing prior to addition of DRB or present at DRB-insensitive genes. Supporting that degradation of pRNAPII S2 occurred after DRB and UV co-treatment, MG132 counteracted this effect (Figure 5B,C compare pRNAPII S2 UV + DRB to UV + DRB + MG132). However, the increase in chromatin levels of pRNAPII S5 was greater than the increase in pRNAPII S2 after the triple treatment with UV + DRB + MG132 compared to UV + DRB, in line with more promoter proximal RNAPII being degraded than elongating RNAPII (Figure 5B, C). Degradation of promoter proximal paused RNAPII thus contributes to regulation of global RNAPII levels on chromatin after UV. Interestingly, DRB also caused a relatively greater reduction in pRNAPII S2 levels in G1 and G2 phase compared to S phase after UV (Figure 5D, E), supporting higher stability of the productively elongating fraction in S phase after UV.

Initiation is required for enhanced proteasome mediated degradation of promoter proximal RNAPII after UV

Enhanced degradation of promoter proximal RNAPII after UV was unanticipated, as this form of RNAPII does not travel very far along the DNA molecule and is thus not expected to encounter much DNA damage directly. In light of our result suggesting that initiation is likely enhanced and leads to more promoter proximal stalling after UV (Figure 2), together with the finding that DRB promoted RNAPII degradation (Figure 4), we hypothesized that the degradation might be triggered by abnormally high levels of promoter proximal stalled RNAPII after UV. To address this, we added THZ1, which inhibits RNAPII at a step prior to promoter proximal pausing (38,48). As expected, THZ1 caused the release of a large fraction of RNAPII from chromatin in all cell cycle phases (Figure 6A–D). However, the levels of pRNAPII S5 on chromatin were not further reduced by UV upon THZ1 treatment (Figure 6B, C). New transcription initiation leading to the production of new

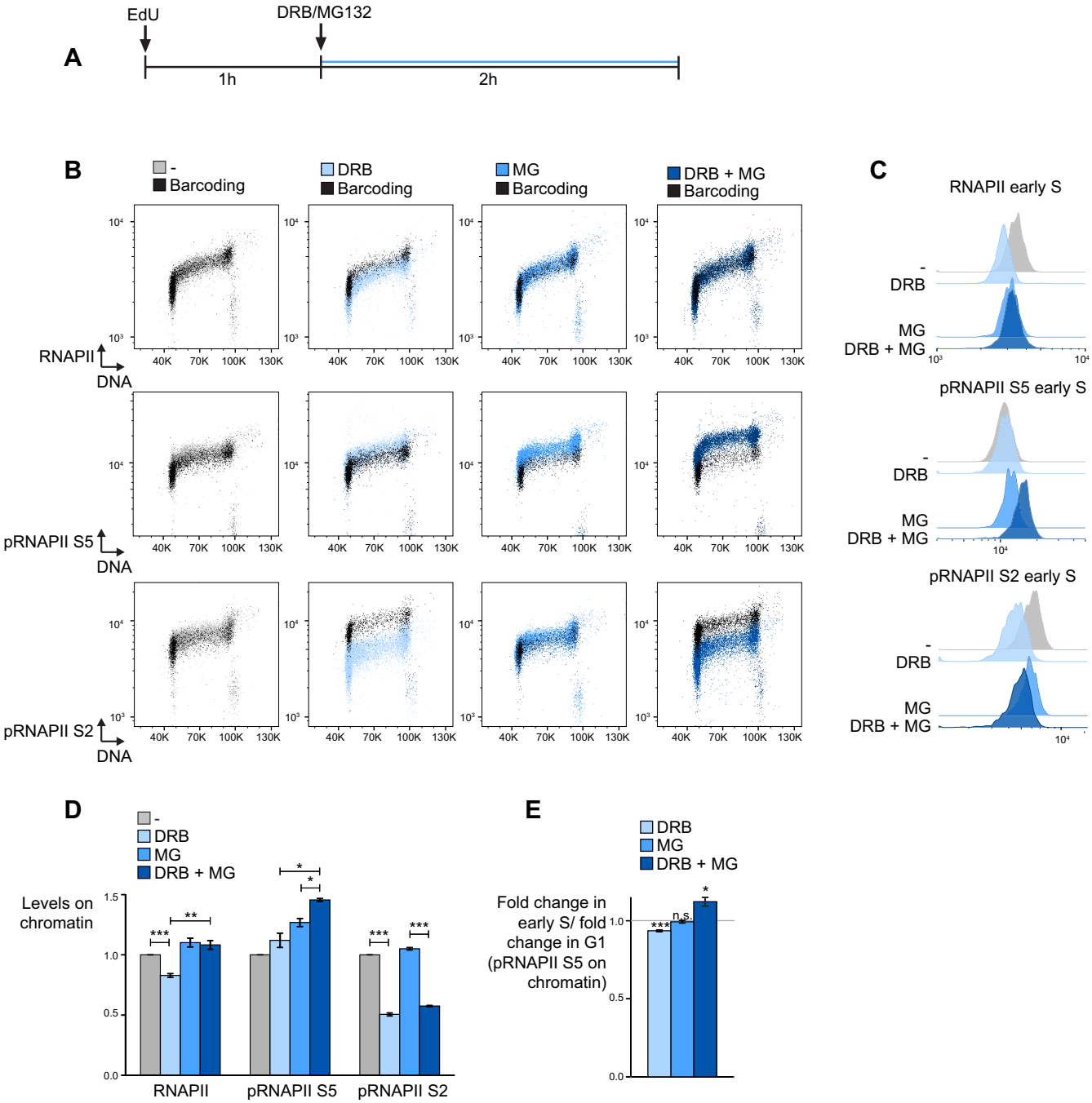

Figure 4. Promoter proximal RNAPII is subjected to proteasome-mediated degradation on chromatin in unperturbed conditions. (**A**) Overview of experimental set up. EdU was added to HeLa cells 1h prior to addition of 100 μM DRB and/or 50 μM MG132. Samples were harvested, extracted and fixed for flow cytometry analysis after 2h. (**B**) Flow cytometry scatter plots showing levels of RNAPII, pRNAPII S5 and pRNAPII S2 on chromatin versus DNA content from samples treated as in (A). Non-treated cells (−) are shown in grey, and samples treated with DRB and/or MG132 are shown in colors as indicated. Barcoded control cells (shown in black) are shown in scatterplots together with the sample cells as in Figure 2B. (**C**) Flow cytometry histograms showing RNAPII, pRNAPII S5 and pRNAPII S2 levels on chromatin vs cell count in individual cells in early S phase treated as in A). (**D**) Mean median RNAPII, pRNAPII S5 and pRNAPII S2 levels on chromatin in cells treated as in (A) and normalized to barcoding cells. Samples treated with DRB and/or MG132 were further normalized to non-treated cells ($n = 3$), significance tested by the two-tailed two sample Student's *t*-test. Error bars represent SEM. (**E**) Mean fold changes after DRB, MG132 and MG132 + DRB treatment in early S cells divided by the mean fold changes in G1 cells. ((chromatin levels in treated/non-treated early S cells)/(chromatin levels in treated/non-treated G1 cells)). With DRB this value goes below 1, meaning pRNAPII S5 is more removed in early S versus G1 phase. With DRB and MG132 the value goes above 1, meaning MG132 treatment increases pRNAPII S5 levels on chromatin more in early S versus G1 cells in the presence of DRB. With MG132 alone this value is equal to 1, showing there is no significant difference in the effect of MG132 in early S versus G1. ($n = 3$), significance tested by the two-tailed two sample Student's *t*-test. Error bars represent SEM.

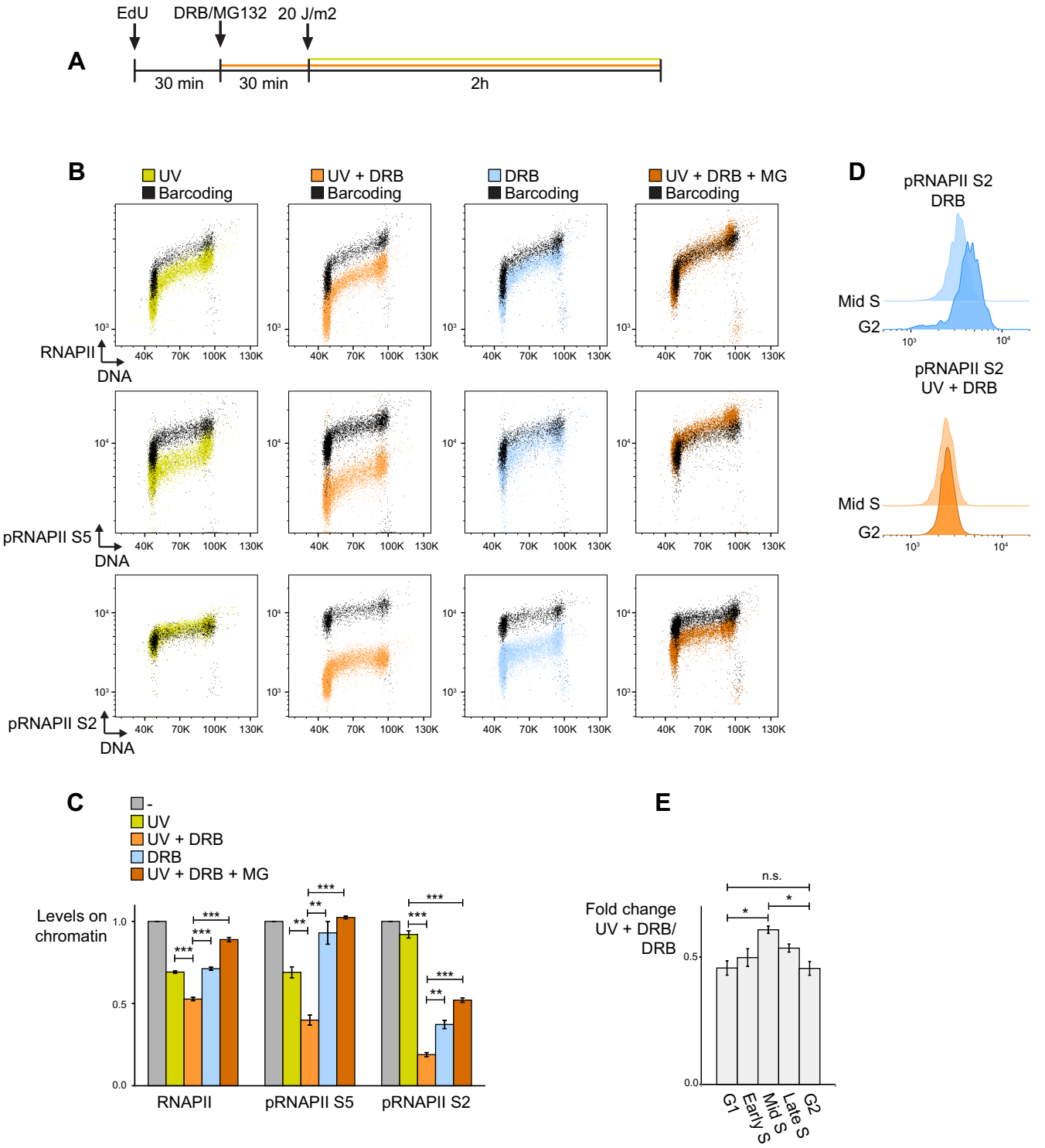

Figure 5. Promoter proximal RNAPII is subjected to proteasome-mediated degradation on chromatin after UV. (**A**) Overview of experimental set up. EdU was added to HeLa cells 30min prior to addition of 100 μM DRB and/or 50 μM MG132. 30min after this, samples were UV irradiated with 20 J/m^2. After 2h, samples were harvested, extracted and fixed for flow cytometry analysis. (**B**) Flow cytometry scatter plots showing levels of RNAPII, pRNAPII S5 and pRNAPII S2 on chromatin versus DNA content from samples treated as in (A). Samples treated with UV, UV + DRB, DRB and UV + DRB + MG132 are shown in colors as indicated. Barcoded control cells (shown in black) are shown in scatterplots together with the sample cells as in Figure 2B. (**C**) Mean median RNAPII, pRNAPII S5 and pRNAPII S2 levels on chromatin in cells treated as in (A) and normalized to barcoding cells. Samples treated with UV or inhibitors were normalized to non-treated sample (−) ($n = 3$), significance tested by the two-tailed two sample Student's *t*-test. Error bars represent SEM. (**D**) Histograms showing RNAPII pS2 levels on chromatin versus cell count in mid S and G2 phases of the cell cycle from the same experiment as in (B). Cell cycle phases were identified based on DNA content and EdU levels, as shown in Figure 1F). (**E**) Mean fold changes of RNAPII pS2 levels on chromatin in UV + DRB-treated cells relative to mean fold changes in DRB-treated cells, from experiments such as in (B). Results are shown for individual phases of the cell cycle. Note that UV reduces pRNAPII S2 levels in chromatin less in S phase in the presence of DRB. ($n = 3$), significance tested by the two-tailed two-sample Student's *t*-test. Error bars represent SEM.

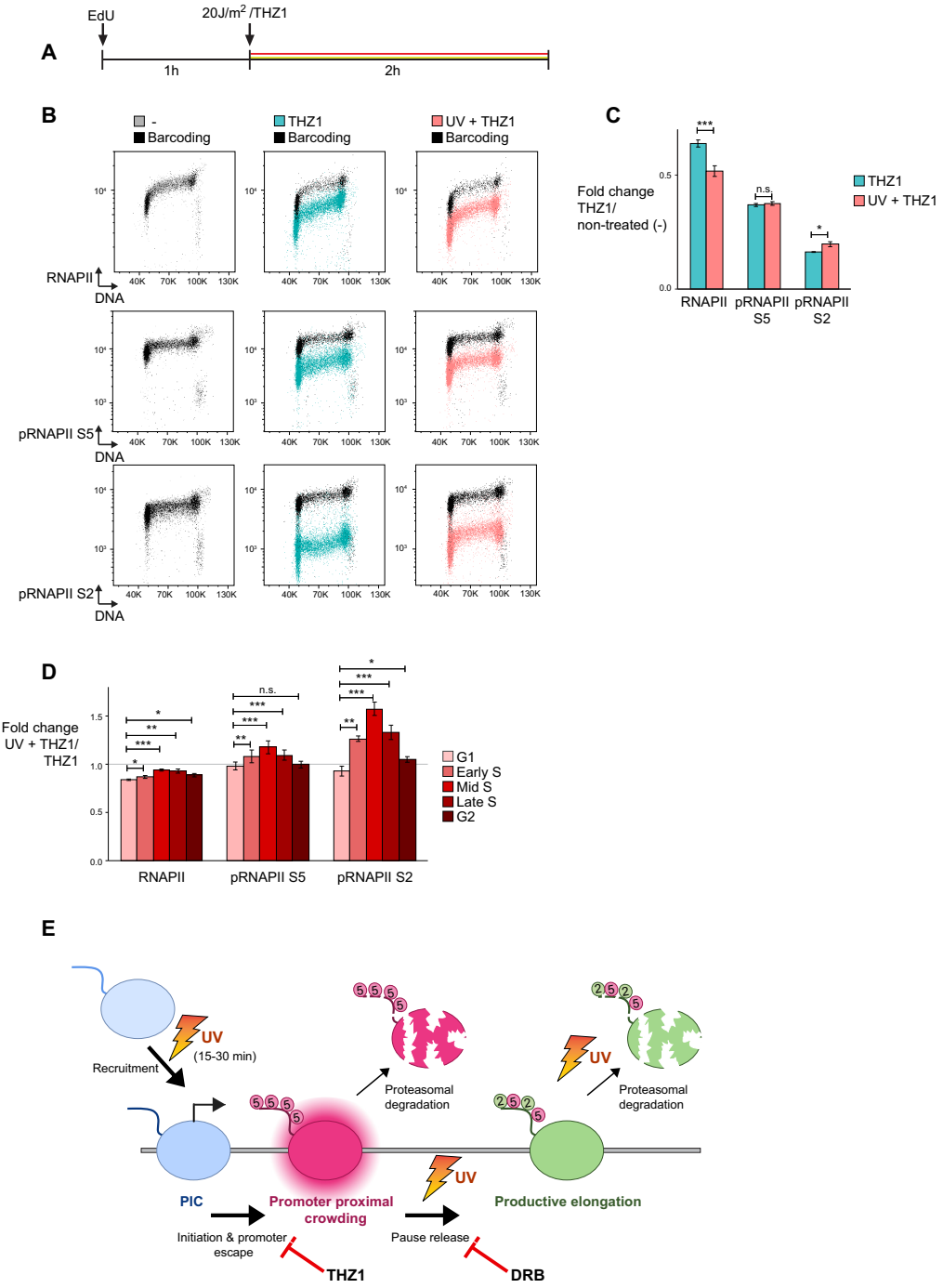

Figure 6. Initiation is required for enhanced proteasome mediated degradation of promoter proximal RNAPII after UV. (**A**) Overview of experimental set up. EdU was added to HeLa cells 1h prior to UV irradiation with 20 J/m^2 and/or addition of 1 μM THZ1 (added directly after UV irradiation). Samples were harvested after 2h, extracted and fixed for flow cytometry analysis. (**B**) Flow cytometry scatter plots showing levels of RNAPII, pRNAPII S5 and pRNAPII S2 on chromatin versus DNA content from samples treated as in A). Non-treated cells (−) are shown in grey, and samples treated with THZ1 +/− UV are shown in colors as indicated. Barcoded control cells (shown in black) are shown in scatterplots together with the sample cells as in Figure 2B. (**C**) Mean fold change after THZ1 +/− UV for RNAPII, pRNAPII S5 and pRNAPII S2 levels on chromatin in cells treated as in A) and normalized to barcoding cells. *(n = 3)*, significance tested by the two-tailed one sample Student's *t*-test. Error bars represent SEM. (**D**) Mean fold changes of RNAPII, pRNAPII S5 and pRNAPII S2 levels on chromatin in UV + THZ1 relative to mean fold changes in THZ1-treated cells. Results are shown for individual phases of the cell cycle (determined as in Figure 1F) ($n = 3$), significance tested by the two-tailed one sample Student's *t*-test. Error bars represent SEM. (**E**) Revised model for the effect of UV on the transcription cycle. Our results suggest that at early timepoints after UV, initiation is enhanced, leading to more promoter proximal stalling. The enhanced promoter proximal stalling causes 'crowding' (see main text for details) around the promoter proximal pause site, pushing RNAPII into productive elongation or degradation (premature termination). Treatment with DRB will exacerbate promoter proximal crowding by preventing pause release, and further enhance degradation of promoter proximal paused RNAPII after UV. THZ1 counteracts crowding at the promoter proximal pause site, as it prevents promoter escape, and thus also UV-induced enhanced degradation. Work by others has shown that UV also enhances pause release (11,33,34,50) and degradation of productively elongating RNAPII (68), which likely directly encounters DNA damage.

promoter proximal RNAPII, is thus likely a requirement for its UV-induced degradation. Indeed, pRNAPII S5 appeared to be slightly more stable after UV in the presence of THZ1, especially in S phase (Figure 6D). Of note, this was similar to pRNAPII S2, which was also slightly more stable in S phase than G1 or G2 phases after UV and THZ1 (Figure 6D). Nevertheless, overall levels of pRNAPII S2 were strongly suppressed by THZ1 in the presence and absence of UV (Figure 6B–D), supporting that continuous initiation followed by release into productive elongation is required for the high pRNAPII S2 levels on chromatin 2h after UV in HeLa cells (Figure 2B–D). Altogether, the results with THZ1 strongly support that the promoter proximal form of RNAPII is being degraded after UV and suggest that the enhanced initiation after UV is required for such degradation.

DISCUSSION

Global regulation of RNAPII levels is involved in transcriptional shutdown, resumption and cell survival after UV (35). So far, the UV-mediated degradation of RNAPII has been thought to involve productively elongating RNAPII (21,41), which is the form that likely encounters DNA damage and participates in TC-NER. Here we show that promoter proximal RNAPII is degraded both in the presence and absence of UV, using a new flow cytometry assay that accurately measures levels of RNAPII, pRNAPII S5 and pRNAPII S2 on chromatin in individual cells through the cell cycle. Inhibiting productive elongation with DRB prior to UV further enhanced degradation of total RNAPII on chromatin, strongly suggesting degradation of promoter proximal RNAPII contributes to regulation of total RNAPII levels after UV. Furthermore, as chromatin loading of RNAPII and pRNAPII S5 were enhanced at early timepoints after UV and suppression of promoter proximal paused RNAPII inhibited UV-mediated degradation of pRNAPII S5 on chromatin, our results suggest enhanced initiation promotes degradation of promoter proximal paused RNAPII at early timepoints after UV. In addition, precise measurements of individual cell cycle transitions revealed that pRNAPII S5 is more degraded after DRB in early S compared to G1 phase in HeLa cells, indicating that transcription replication conflicts are resolved by degradation of promoter proximal RNAPII. On the other hand, pRNAPII S2, associated with productive elongation, was more stable in S phase after UV. As processing of DNA damage-stalled RNAPII is tightly linked to repair (49), the latter may indicate cell cycle specific differences in TC-NER.

Based on the work shown here, we propose a modified model for the effect of UV on transcription (Figure 6E). At early timepoints (15–30min) UV enhances initiation, which leads to more promoter proximal pausing and subsequent elongation. However, as the rate of release into productive elongation is lower than the rate of initiation, UV may cause 'crowding' of RNAPII molecules around the promoter proximal pause site, leading to degradation of promoter proximal paused RNAPII. Inhibiting release into productive elongation by DRB further enhances 'promoter proximal crowding', and increases degradation of promoter proximal RNAPII after UV. Vice versa, suppressing 'promoter proximal crowding' with THZ1 suppresses UV-induced degradation of pRNAPII S5. Notably, increased release from promoter proximal pausing into productive elongation is known to occur after UV (11,33,34,50), but is not conflicting with our model as we simply propose that, at early timepoints after UV, the global rate of initiation vs release into productive elongation is higher causing an accumulation of promoter proximal RNAPII on chromatin. Importantly, the rate of release into productive elongation may still be higher compared to non-UV treated cells. 'Promoter proximal crowding', described here, shares similarity with the previously described 'transcription traffic jam' shown to occur behind RNAPII molecules stalled at DNA damage sites (49). However, in gene-internal regions the stretches of DNA are larger, and can encompass more molecules. From the pre-initiation complex to the promoter proximal pause site there is only ∼47 bp (51). As RNAPII occupies ∼33 bp (52), there is simply not room for a queue. Thus, though conceptually related, 'promoter proximal crowding' is not the same as a 'transcription traffic jam'.

Degradation of RNAPII at the promoter proximal pause site, as shown here, necessarily involves premature termination. A major implication of our work is thus that premature termination, which frequently occurs at the promoter proximal pause site (16,53,54), likely also involves RNAPII degradation on chromatin. Of note, previous reports have not observed enhanced degradation of RNAPII after DRB and UV (55,56). However, a major difference is that these studies measured RNAPII levels in whole cell lysates (55,56), while we measure the chromatin bound fraction in individual cells, used different antibodies and accurate quantification including the barcoding approach. The phospho-specific antibodies used here have been tested in vitro to detect pRNAPII S2 and S5 (57). Moreover, in this work we have used pRNAPII S5 as a marker for promoter proximal RNAPII. It is well established and easily observed in ChIP experiments that the majority of the pRNAPII S5 signal during normal transcription derives from promoter proximal pausing (58). Nevertheless, this does not exclude a role for pRNAPII S5 downstream of promoter proximal pause sites. Indeed, pRNAPII S5 plays a role at splice sites (59), and is found within 8 kb of transcriptional start sites of poised genes (60). After UV and THZ1 treatment, a small fraction of pRNAPII S5 was more stable in S phase (Figure 6). This is reminiscent of the more stable fraction of elongating pRNAPII S2 in S phase after UV, in line with this fraction being dually phosphorylated on S2 and S5. As pRNAPII S5 has been reported to be refractory to degradation (21), this may indicate that promoter proximal paused RNAPII and productively elongating RNAPII may be degraded by different pathways, and that pRNAPII S5 may play different roles in these.

Our results suggest initiation is enhanced after UV leading to more promoter proximal pausing at early timepoints. Notably, most previous work has dealt with later timepoints after UV. However, one study showed global hyperphosphorylation of RNAPII at 1h after UV by western blotting (61) which is consistent with enhanced initiation, as RNAPII becomes phosphorylated during the first steps of transcription (20). Furthermore, RNA synthesis from

all transcription start sites was higher at 1h after UV by nRNA-seq (33), also in line with enhanced initiation. In addition, enhanced promoter proximal stalling after UV is supported by the redistribution of RNA reads toward the 5′ ends of genes upon labeling 0-45min after UV by BruUV-seq (62) and TT-seq (35). Nevertheless, the common view is that UV downregulates transcription initiation (63). In line with the latter, RNAPII levels at transcription start sites were lower at 1.5h after UV by ChIP-seq (33), and RNA reads were reduced at promoter proximal sites at 2h after UV by GRO-seq (11) and at 3h after UV by TT-seq (35). Notably, downregulation of transcription initiation after UV is thought to occur via reduction of the global RNAPII pool by proteasome-mediated degradation of elongating RNAPII (35), and by enhanced expression of the early response gene ATF3 (64), both of which take some time to occur. We therefore propose that the findings can be reconciled by separating the effects after UV into early response (<1h), where initiation and promoter proximal pausing are enhanced, and late response (>1h), where they are suppressed. Such a hypothesis fits well with our results, as RNAPII and pRNAPII S5 loading were enhanced at 15–30min, but reduced at 2h after UV (Figure 2).

The effect of the cell cycle on RNAPII chromatin binding after UV has been little studied, likely because, until now, a good technique to study this has been lacking. Overall, UV induced changes on RNAPII chromatin binding occurred globally in all cell cycle phases. However, cell cycle specific effects could still be detected. As RNAPII processing is tightly linked to TC-NER in human cells (49), the most relevant cell cycle effect with regard to DNA repair is likely the higher stability of elongating RNAPII in S phase after UV. Though TC-NER can occur throughout most of the cell cycle, several of the factors required for the later steps of NER are shared with replication and are expressed in a cell cycle dependent manner (65). Moreover, another cell cycle difference we observed in this work is the enhanced degradation of pRNAPII S5 in S phase compared to G1 or G2 phases after UV in HeLa cells (Figure 2). Furthermore, more pRNAPII S5 was degraded on chromatin in early S phase compared to G1 phase after DRB (Figure 4). This suggests promoter proximal degradation of RNAPII is promoted by replication. Degradation of promoter proximal RNAPII may thus be a mechanism by which the cells deals with collisions between promoter proximal paused RNAPII and replication. Such a mechanism is likely important, as promoter proximal RNAPII can be stable for ∼1h (66).

An advantage of flow cytometry versus other available techniques is statistical strength, which is due to the measurement of thousands of individual cells per sample per experiment. In addition, flow cytometry is rapid, and multiparameter data processing is highly feasible. As it provides an internal control in each sample for normalization, including barcoding greatly facilitates quantifications and sensitivity. The barcoded cells are divided, mixed and stained with each of the samples, so that sample to sample variation during staining is eliminated. Furthermore, EdU incorporation and pH3S10 staining allows the study of RNAPII levels in different cycle phases without having to synchronize cells. It also adds another layer of accuracy, as the contribution of e.g. replication can be specified. This is illustrated in Supplementary Figure S2A, where enhanced levels of RNAPII were detected on chromatin in G1, but not in S phase cells at 30min after UV. Furthermore, in our assay, cells were extracted prior to fixation, causing the release of un- or weakly bound proteins from chromatin. Confirming the accuracy of our method, mitotic cells showed similarly low levels of chromatin binding of RNAPII and its phosphorylated forms by flow cytometry as by western blotting. Several other transcription-related proteins are also released from chromatin in mitosis (26,67), and lower mitotic staining can thus likely be used to verify the accuracy of flow cytometry chromatin binding assays for other proteins as well. This method may further be useful to study mitotic repression of transcription at the G2/M transition. Indeed we found that high mitotic pH3S10 levels occurs prior to the release of RNAPII from chromatin at the G2/M transition (Figure 1), in agreement with another study which found that nascent transcription can be observed in pH3S10 positive cells in early prophase (24). Moreover, using transcriptional inhibitors, we also show that this method can be used to study the transcription cycle itself. Notably, DRB, a well-known inhibitor of release from promoter proximal pausing (42), maintained levels of pRNAPII S5 while strongly suppressing pRNAPII S2. On the other hand, THZ1, which inhibits the transition from initiation into promoter proximal pausing (38), as expected lowered the levels of both pRNAPII S5 and pRNAPII S2.

All in all, here we have developed a rapid, highly sensitive and quantitative assay to study chromatin binding of RNAPII and its phosphorylated forms through the cell cycle. In combination with transcriptional and proteasome inhibitors it can be used to study the transcription cycle and follow the fate of RNAPII on chromatin. Using this method we show that elongating RNAPII becomes more stable in S phase after UV, suggesting cell cycle specific effects in TC-NER. Furthermore, we show that promoter proximal RNAPII is degraded on chromatin in the absence and presence of UV DNA damage, and propose a new modified model for the effect of UV on the transcription cycle. Our results suggest degradation of promoter proximal paused RNAPII substantially contributes to the regulation of the 'RNAPII pool', and may thus be important for transcription resumption and cell survival after UV.

DATA AVAILABILITY

The data has been deposited to the FLOW repository (https://flowrepository.org/) with IDs: FR-FCM-Z5CR, FR-FCM-Z5CE, FR-FCM-Z5CQ, FR-FCM-Z5CX and FR-FCM-Z5CP.

SUPPLEMENTARY DATA

Supplementary Data are available at NAR Online.

ACKNOWLEDGEMENTS

We are grateful for assistance and use of the flow cytometry core facility at the Radium Hospital, Oslo University Hospital.

FUNDING

Norwegian Research Council [275918]. Funding for open access charge: Norwegian Research Council [275918].
Conflict of interest statement. None declared.

REFERENCES

1. Tudek,A., Candelli,T. and Libri,D. (2015) Non-coding transcription by RNA polymerase II in yeast: Hasard or nécessité? *Biochimie*, **117**, 28–36.
2. Gaul,L. and Svejstrup,J.Q. (2021) Transcription-coupled repair and the transcriptional response to UV-Irradiation. *DNA Repair (Amst.)*, **107**, 103208.
3. Lesage,E., Clouaire,T. and Legube,G. (2021) Repair of DNA double-strand breaks in RNAPI- and RNAPII-transcribed loci. *DNA Repair (Amst.)*, **104**, 103139.
4. Montaldo,N.P., Bordin,D.L., Brambilla,A., Rösinger,M., Fordyce Martin,S.L., Bjørås,K., Bradamante,S., Aas,P.A., Furrer,A., Olsen,L.C. *et al.* (2019) Alkyladenine DNA glycosylase associates with transcription elongation to coordinate DNA repair with gene expression. *Nat. Commun.*, **10**, 5460.
5. Enoiu,M., Jiricny,J. and Schärer,O.D. (2012) Repair of cisplatin-induced DNA interstrand crosslinks by a replication-independent pathway involving transcription-coupled repair and translesion synthesis. *Nucleic Acids Res.*, **40**, 8953–8964.
6. Mulderrig,L., Garaycoechea,J.I., Tuong,Z.K., Millington,C.L., Dingler,F.A., Ferdinand,J.R., Gaul,L., Tadross,J.A., Arends,M.J., O'Rahilly,S. *et al.* (2021) Aldehyde-driven transcriptional stress triggers an anorexic DNA damage response. *Nature*, **600**, 158–163.
7. Landsverk,H.B., Sandquist,L.E., Sridhara,S.C., Rødland,G.E., Sabino,J.C., de Almeida,S.F., Grallert,B., Trinkle-Mulcahy,L. and Syljuåsen,R.G. (2019) Regulation of ATR activity via the RNA polymerase II associated factors CDC73 and PNUTS-PP1. *Nucleic Acids Res.*, **47**, 1797–1813.
8. Lindsey-Boltz,L.A. and Sancar,A. (2007) RNA polymerase: the most specific damage recognition protein in cellular responses to DNA damage? *Proc. Nat. Acad. Sci. U.S.A.*, **104**, 13213–13214.
9. Jackson,S.P. and Bartek,J. (2009) The DNA-damage response in human biology and disease. *Nature*, **461**, 1071–1078.
10. Lans,H., Hoeijmakers,J.H.J., Vermeulen,W. and Marteijn,J.A. (2019) The DNA damage response to transcription stress. *Nat. Rev.*, **20**, 766–784.
11. Williamson,L., Saponaro,M., Boeing,S., East,P., Mitter,R., Kantidakis,T., Kelly,G.P., Lobley,A., Walker,J., Spencer-Dene,B. *et al.* (2017) UV irradiation induces a Non-coding RNA that functionally opposes the protein encoded by the same gene. *Cell*, **168**, 843–855.
12. Mayne,L.V. and Lehmann,A.R. (1982) Failure of RNA synthesis to recover after UV irradiation: an early defect in cells from individuals with Cockayne's syndrome and xeroderma pigmentosum. *Cancer Res.*, **42**, 1473–1478.
13. Ratner,J.N., Balasubramanian,B., Corden,J., Warren,S.L. and Bregman,D.B. (1998) Ultraviolet radiation-induced ubiquitination and proteasomal degradation of the large subunit of RNA polymerase II. Implications for transcription-coupled DNA repair. *J. Biol. Chem.*, **273**, 5184–5189.
14. Woudstra,E.C., Gilbert,C., Fellows,J., Jansen,L., Brouwer,J., Erdjument-Bromage,H., Tempst,P. and Svejstrup,J.Q. (2002) A Rad26-Def1 complex coordinates repair and RNA pol II proteolysis in response to DNA damage. *Nature*, **415**, 929–933.
15. Core,L. and Adelman,K. (2019) Promoter-proximal pausing of RNA polymerase II: a nexus of gene regulation. *Genes Dev.*, **33**, 960–982.
16. Contreras,X., Benkirane,M. and Kiernan,R. (2013) Premature termination of transcription by RNAP II: the beginning of the end. *Transcription*, **4**, 72–76.
17. Jensen,T.H., Jacquier,A. and Libri,D. (2013) Dealing with pervasive transcription. *Mol. Cell*, **52**, 473–484.
18. Eaton,J.D. and West,S. (2020) Termination of transcription by RNA polymerase II: BOOM! *Trends Genet.: TIG*, **36**, 664–675.
19. Cossa,G., Parua,P.K., Eilers,M. and Fisher,R.P. (2021) Protein phosphatases in the RNAPII transcription cycle: erasers, sculptors, gatekeepers, and potential drug targets. *Genes Dev.*, **35**, 658–676.
20. Harlen,K.M. and Churchman,L.S. (2017) The code and beyond: transcription regulation by the RNA polymerase II carboxy-terminal domain. *Nat. Rev.*, **18**, 263–273.
21. Somesh,B.P., Reid,J., Liu,W.F., Sogaard,T.M., Erdjument-Bromage,H., Tempst,P. and Svejstrup,J.Q. (2005) Multiple mechanisms confining RNA polymerase II ubiquitylation to polymerases undergoing transcriptional arrest. *Cell*, **121**, 913–923.
22. Yasukawa,T., Kamura,T., Kitajima,S., Conaway,R.C., Conaway,J.W. and Aso,T. (2008) Mammalian Elongin a complex mediates DNA-damage-induced ubiquitylation and degradation of Rpb1. *EMBO J.*, **27**, 3256–3266.
23. Delgado-Román,I. and Muñoz-Centeno,M.C. (2021) Coupling between cell cycle progression and the nuclear RNA polymerases system. *Front. Mol. Biosci.*, **8**, 691636.
24. Liang,K., Woodfin,A.R., Slaughter,B.D., Unruh,J.R., Box,A.C., Rickels,R.A., Gao,X., Haug,J.S., Jaspersen,S.L. and Shilatifard,A. (2015) Mitotic transcriptional activation: clearance of actively engaged Pol II via transcriptional elongation control in mitosis. *Mol. Cell*, **60**, 435–445.
25. Gottesfeld,J.M. and Forbes,D.J. (1997) Mitotic repression of the transcriptional machinery. *Trends Biochem. Sci*, **22**, 197–202.
26. Martínez-Balbás,M.A., Dey,A., Rabindran,S.K., Ozato,K. and Wu,C. (1995) Displacement of sequence-specific transcription factors from mitotic chromatin. *Cell*, **83**, 29–38.
27. Gomez-Gonzalez,B. and Aguilera,A. (2019) Transcription-mediated replication hindrance: a major driver of genome instability. *Genes Dev.*, **33**, 1008–1026.
28. Poli,J., Gerhold,C.B., Tosi,A., Hustedt,N., Seeber,A., Sack,R., Herzog,F., Pasero,P., Shimada,K., Hopfner,K.P. *et al.* (2016) Mec1, INO80, and the PAF1 complex cooperate to limit transcription replication conflicts through RNAPII removal during replication stress. *Genes Dev.*, **30**, 337–354.
29. Landsverk,H.B., Sandquist,L.E., Bay,L.T.E., Steurer,B., Campsteijn,C., Landsverk,O.J.B., Marteijn,J.A., Petermann,E., Trinkle-Mulcahy,L. and Syljuåsen,R.G. (2020) WDR82/PNUTS-PP1 prevents transcription–replication conflicts by promoting RNA polymerase II degradation on chromatin. *Cell Rep.*, **33**, 108469.
30. Wang,J., Rojas,P., Mao,J., Mustè Sadurnì,M., Garnier,O., Xiao,S., Higgs,M.R., Garcia,P. and Saponaro,M. (2021) Persistence of RNA transcription during DNA replication delays duplication of transcription start sites until G2/M. *Cell Rep.*, **34**, 108759.
31. Rudé,J.M. and Friedberg,E.C. (1977) Semi-conservative deoxyribonucleic acid synthesis in unirradiated and ultraviolet-irradiated xeroderma pigmentosum and normal human skin fibroblasts. *Mutat. Res.*, **42**, 433–442.
32. Mailand,N., Falck,J., Lukas,C., Syljuåsen,R.G., Welcker,M., Bartek,J. and Lukas,J. (2000) Rapid destruction of human Cdc25A in response to DNA damage. *Science (New York, N.Y.)*, **288**, 1425–1429.
33. Liakos,A., Konstantopoulos,D., Lavigne,M.D. and Fousteri,M. (2020) Continuous transcription initiation guarantees robust repair of all transcribed genes and regulatory regions. *Nat. Commun.*, **11**, 916.
34. Lavigne,M.D., Konstantopoulos,D., Ntakou-Zamplara,K.Z., Liakos,A. and Fousteri,M. (2017) Global unleashing of transcription elongation waves in response to genotoxic stress restricts somatic mutation rate. *Nat. Commun.*, **8**, 2076.
35. Tufegdžić Vidaković,A., Mitter,R., Kelly,G.P., Neumann,M., Harreman,M., Rodríguez-Martínez,M., Herlihy,A., Weems,J.C., Boeing,S., Encheva,V. *et al.* (2020) Regulation of the RNAPII pool is integral to the DNA damage response. *Cell*, **180**, 1245–1261.
36. Boeing,S., Williamson,L., Encheva,V., Gori,I., Saunders,R.E., Instrell,R., Aygun,O., Rodriguez-Martinez,M., Weems,J.C., Kelly,G.P. *et al.* (2016) Multiomic analysis of the UV-Induced DNA damage response. *Cell Rep.*, **15**, 1597–1610.
37. Geijer,M.E., Zhou,D., Selvam,K., Steurer,B., Mukherjee,C., Evers,B., Cugusi,S., van Toorn,M., van der Woude,M., Janssens,R.C. *et al.* (2021) Elongation factor ELOF1 drives transcription-coupled repair and prevents genome instability. *Nat. Cell Biol.*, **23**, 608–619.
38. Steurer,B., Janssens,R.C., Geverts,B., Geijer,M.E., Wienholz,F., Theil,A.F., Chang,J., Dealy,S., Pothof,J., van Cappellen,W.A. *et al.* (2018) Live-cell analysis of endogenous GFP-RPB1 uncovers rapid turnover of initiating and promoter-paused RNA polymerase II. *Proc. Nat. Acad. Sci. U.S.A.*, **115**, E4368–E4376.

39. Håland,T.W., Boye,E., Stokke,T., Grallert,B. and Syljuåsen,R.G. (2015) Simultaneous measurement of passage through the restriction point and MCM loading in single cells. *Nucleic Acids Res.*, **43**, e150.
40. Parsons,G.G. and Spencer,C.A. (1997) Mitotic repression of RNA polymerase II transcription is accompanied by release of transcription elongation complexes. *Mol. Cell. Biol.*, **17**, 5791–5802.
41. Noe Gonzalez,M., Blears,D. and Svejstrup,J.Q. (2021) Causes and consequences of RNA polymerase II stalling during transcript elongation. *Nat. Rev.*, **22**, 3–21.
42. Yamaguchi,Y., Shibata,H. and Handa,H. (2013) Transcription elongation factors DSIF and NELF: promoter-proximal pausing and beyond. *Biochim. Biophys. Acta*, **1829**, 98–104.
43. Salifou,K., Burnard,C., Basavarajaiah,P., Grasso,G., Helsmoortel,M., Mac,V., Depierre,D., Franckhauser,C., Beyne,E., Contreras,X. *et al.* (2021) Chromatin-associated MRN complex protects highly transcribing genes from genomic instability. *Sci. Adv.*, **7**, eabb2947.
44. Sheridan,R.M., Fong,N., D'Alessandro,A. and Bentley,D.L. (2019) Widespread backtracking by RNA Pol II is a major effector of gene activation, 5′ pause release, termination, and transcription elongation rate. *Mol. Cell*, **73**, 107–118.
45. Erickson,B., Sheridan,R.M., Cortazar,M. and Bentley,D.L. (2018) Dynamic turnover of paused Pol II complexes at human promoters. *Genes Dev.*, **32**, 1215–1225.
46. Gomes,N.P., Bjerke,G., Llorente,B., Szostek,S.A., Emerson,B.M. and Espinosa,J.M. (2006) Gene-specific requirement for P-TEFb activity and RNA polymerase II phosphorylation within the p53 transcriptional program. *Genes Dev.*, **20**, 601–612.
47. Pope,B.D., Hiratani,I. and Gilbert,D.M. (2010) Domain-wide regulation of DNA replication timing during mammalian development. *Chromosome Res.*, **18**, 127–136.
48. Nilson,K.A., Guo,J., Turek,M.E., Brogie,J.E., Delaney,E., Luse,D.S. and Price,D.H. (2015) THZ1 reveals roles for Cdk7 in Co-transcriptional capping and pausing. *Mol. Cell*, **59**, 576–587.
49. Nakazawa,Y., Hara,Y., Oka,Y., Komine,O., van den Heuvel,D., Guo,C., Daigaku,Y., Isono,M., He,Y., Shimada,M. *et al.* (2020) Ubiquitination of DNA damage-stalled RNAPII promotes transcription-coupled repair. *Cell*, **180**, 1228–1244.
50. Studniarek,C., Tellier,M., Martin,P.G.P., Murphy,S., Kiss,T. and Egloff,S. (2021) The 7SK/P-TEFb snRNP controls ultraviolet radiation-induced transcriptional reprogramming. *Cell Rep.*, **35**, 108965.
51. Shao,W. and Zeitlinger,J. (2017) Paused RNA polymerase II inhibits new transcriptional initiation. *Nat. Genet.*, **49**, 1045–1051.
52. Saeki,H. and Svejstrup,J.Q. (2009) Stability, flexibility, and dynamic interactions of colliding RNA polymerase II elongation complexes. *Mol. Cell*, **35**, 191–205.
53. Brannan,K., Kim,H., Erickson,B., Glover-Cutter,K., Kim,S., Fong,N., Kiemele,L., Hansen,K., Davis,R., Lykke-Andersen,J. *et al.* (2012) mRNA decapping factors and the exonuclease Xrn2 function in widespread premature termination of RNA polymerase II transcription. *Mol. Cell*, **46**, 311–324.
54. Wagschal,A., Rousset,E., Basavarajaiah,P., Contreras,X., Harwig,A., Laurent-Chabalier,S., Nakamura,M., Chen,X., Zhang,K., Meziane,O. *et al.* (2012) Microprocessor, Setx, Xrn2, and Rrp6 co-operate to induce premature termination of transcription by RNAPII. *Cell*, **150**, 1147–1157.
55. Luo,Z., Zheng,J., Lu,Y. and Bregman,D.B. (2001) Ultraviolet radiation alters the phosphorylation of RNA polymerase II large subunit and accelerates its proteasome-dependent degradation. *Mutat. Res.*, **486**, 259–274.
56. McKay,B.C., Chen,F., Clarke,S.T., Wiggin,H.E., Harley,L.M. and Ljungman,M. (2001) UV light-induced degradation of RNA polymerase II is dependent on the Cockayne's syndrome A and B proteins but not p53 or MLH1. *Mutat. Res.*, **485**, 93–105.
57. Chapman,R.D., Heidemann,M., Albert,T.K., Mailhammer,R., Flatley,A., Meisterernst,M., Kremmer,E. and Eick,D. (2007) Transcribing RNA polymerase II is phosphorylated at CTD residue serine-7. *Science (New York, N.Y.)*, **318**, 1780–1782.
58. Heidemann,M., Hintermair,C., Voss,K. and Eick,D. (2013) Dynamic phosphorylation patterns of RNA polymerase II CTD during transcription. *Biochim. Biophys. Acta*, **1829**, 55–62.
59. Nojima,T., Rebelo,K., Gomes,T., Grosso,A.R., Proudfoot,N.J. and Carmo-Fonseca,M. (2018) RNA polymerase II phosphorylated on CTD serine 5 interacts with the spliceosome during Co-transcriptional splicing. *Mol. Cell*, **72**, 369–379.
60. Brookes,E. and Pombo,A. (2009) Modifications of RNA polymerase II are pivotal in regulating gene expression states. *EMBO Rep.*, **10**, 1213–1219.
61. Rockx,D.A., Mason,R., van Hoffen,A., Barton,M.C., Citterio,E., Bregman,D.B., van Zeeland,A.A., Vrieling,H. and Mullenders,L.H. (2000) UV-induced inhibition of transcription involves repression of transcription initiation and phosphorylation of RNA polymerase II. *Proc. Nat. Acad. Sci. U.S.A.*, **97**, 10503–10508.
62. Andrade-Lima,L.C., Veloso,A., Paulsen,M.T., Menck,C.F. and Ljungman,M. (2015) DNA repair and recovery of RNA synthesis following exposure to ultraviolet light are delayed in long genes. *Nucleic Acids Res.*, **43**, 2744–2756.
63. van den Heuvel,D., van der Weegen,Y., Boer,D.E.C., Ogi,T. and Luijsterburg,M.S. (2021) Transcription-Coupled DNA repair: from mechanism to human disorder. *Trends Cell Biol.*, **31**, 359–371.
64. Kristensen,U., Epanchintsev,A., Rauschendorf,M.A., Laugel,V., Stevnsner,T., Bohr,V.A., Coin,F. and Egly,J.M. (2013) Regulatory interplay of Cockayne syndrome B ATPase and stress-response gene ATF3 following genotoxic stress. *Proc. Nat. Acad. Sci. U.S.A.*, **110**, E2261–E2270.
65. Mjelle,R., Hegre,S.A., Aas,P.A., Slupphaug,G., Drabløs,F., Saetrom,P. and Krokan,H.E. (2015) Cell cycle regulation of human DNA repair and chromatin remodeling genes. *DNA Repair (Amst.)*, **30**, 53–67.
66. Chen,F., Gao,X. and Shilatifard,A. (2015) Stably paused genes revealed through inhibition of transcription initiation by the TFIIH inhibitor triptolide. *Genes Dev.*, **29**, 39–47.
67. Muchardt,C., Reyes,J.C., Bourachot,B., Leguoy,E. and Yaniv,M. (1996) The hbrm and BRG-1 proteins, components of the human SNF/SWI complex, are phosphorylated and excluded from the condensed chromosomes during mitosis. *EMBO J.*, **15**, 3394–3402.
68. Wilson,M.D., Harreman,M. and Svejstrup,J.Q. (2013) Ubiquitylation and degradation of elongating RNA polymerase II: the last resort. *Biochim. Biophys. Acta*, **1829**, 151–157.